

Keles, H. O., Barbour, R. L., and Omurtag, A. (2016). Hemodynamic correlates of spontaneous neural activity measured by human whole-head resting state EEG+fNIRS. *Neuroimage* 138, 78–87.
doi:10.1016/j.neuroimage.2016.05.058

HEMODYNAMIC CORRELATES OF SPONTANEOUS NEURAL ACTIVITY MEASURED BY HUMAN WHOLE-HEAD RESTING STATE EEG+fNIRS

Hasan Onur Keles ^a, Randall L. Barbour ^b, Ahmet Omurtag ^a

^a Department of Biomedical Engineering, University of Houston, Houston, TX, 77204

^b Department of Pathology, Optical Tomography Group, State University of New York, NY,
11203

* Corresponding author: Ahmet Omurtag, PhD

Tel: 713-743-4484 Fax: 713-743-0226

E-mail address: aomurtag@uh.edu

Keywords: Simultaneous EEG+fNIRS, Resting State, Neurovascular Coupling

ABSTRACT

The brains of awake, resting human subjects display spontaneously occurring neural activity patterns whose magnitude is typically many times greater than those triggered by cognitive or perceptual performance. Such resting state (RS) activity is thought to reflect the functional organization of the brain. In addition, both evoked and RS activation affect local cerebral hemodynamic properties through processes collectively referred to as neurovascular coupling. This is a major topic of interest due to its relationship with pathological conditions that include hypertension, stroke, subarachnoid hemorrhage, and traumatic brain injury. Its investigation calls for an ability to track both the neural and vascular aspects of brain function. We used scalp electroencephalography (EEG), which provided a measure of the electrical potentials generated by cortical postsynaptic currents. Simultaneously we utilized functional near-infrared spectroscopy (NIRS) to continuously monitor hemoglobin concentration changes in superficial cortical layers. The multi-modal signal from 18 healthy adult subjects allowed us to investigate the association of neural activity in a range of frequencies over the whole-head to local changes in hemoglobin concentrations. Our results verified the delayed alpha (8-16 Hz) modulation of hemodynamics in posterior areas known from the

literature. They also indicated strong beta (16-32 Hz) modulation of hemodynamics. Analysis revealed, however, that beta modulation was likely generated by the alpha-beta coupling in EEG. Signals from the inferior electrode sites were dominated by scalp muscle related activity. Our study aimed to characterize the phenomena related to neurovascular coupling observable by practical, cost-effective, and non-invasive multi-modal techniques.

INTRODUCTION

Resting state (RS) electroencephalography (EEG) contains spontaneously occurring patterns with characteristic frequencies and regions on the scalp. These patterns are presumably associated with transient neuronal assemblies that perform various functions linked to information processing (Buzsáki and Draguhn, 2004; Llinas et al., 1998). Among the most studied frequency bands is the alpha rhythm in the range 8-16 Hz. Easily identifiable in the occipital and parietal areas of awake, eyes-closed subjects, it was the first EEG pattern to be observed (Berger, 1929). In addition combinations of delta, theta, alpha, beta, and gamma bands have been reported sometimes coexisting and competing in the same area (Mantini et al., 2007; Steriade, 2001, 2006; Varela et al., 2001) and correlated with RS networks (Laufs et al., 2003; Tyvaert et al., 2008). In fact the distribution of the citations of research on EEG frequency bands replicates the power spectrum of the EEG (Dalal et al., 2011).

EEG is thought to result primarily from the synchronization of post-synaptic potentials and therefore represent the input to a neuronal population rather than its output in the form of action potentials (Buzsáki et al., 2012). Although the underlying process has a time scale on the order of milliseconds, the parts of scalp EEG that are informative about cortical activity generally

remain below the gamma frequency range. This is mainly due to interference from muscle electrical activity (Goncharova et al., 2003; Muthukumaraswamy, 2013; Whitham et al., 2007).

Scalp EEG rhythms have long been used by clinical neurophysiologists in the differential diagnosis of neurological patients (Greenfield et al., 2012; Schomer and Da Silva, 2012). However it is well known that EEG interpretation contains a substantial intuitive component and the accuracy of EEG interpretation is demonstrably low (Grant et al., 2014). These may well be due to our incomplete knowledge of its underlying mechanisms. An important limitation of EEG lies in the difficulty of resolving and spatially localizing its sources (Srinivasan et al., 2007). In order to help overcome such limitations and clarify the relationship of EEG to normal and pathological brain function, researchers are increasingly using multi-modal measurements which combine EEG with other methods.

EEG combined with functional magnetic resonance imaging (fMRI) is able to correlate neural activity with a sequence of highly space-resolved images ultimately based on hemodynamics (Britz et al., 2010; Goldman et al., 2002; Goncalves et al., 2006; Huster et al., 2012; Pouliot, 2012; Sadaghiani et al., 2010). Technical progress has also made it possible to combine EEG with functional NIRS (fNIRS), another non-invasive method. This method, we refer to as EEG+fNIRS, yields similar measurements with lower space but higher time resolution, in a far more practical and cost-effective arrangement (Buccino et al., 2016; Giacometti and Diamond, 2013; Keles et al., 2014; Koch et al., 2006, 2008, 2009; Roche-Labarbe et al., 2008; Safaie et al., 2013). The utility of fNIRS as an independent modality for investigating the adult brain hemodynamics (Gentili et al., 2013; Mesquita et al., 2010; White et al., 2009) as well as infant development (Lloyd-Fox et al., 2010) is already well established. In most fNIRS studies the use of two distinct wavelengths allows the extraction of the concentration changes of oxy- and deoxy-hemoglobin (HbO and HbR) in the outer layers of the cortex (Durduran, 2010;

Scholkmann et al., 2014; Uglialoro, 2014). Following neural activation local blood flow and volume typically increase on a time scale of seconds, causing a rise in HbO and a decrease in HbR of smaller magnitude. These concentration changes measured by fNIRS closely agree with the blood oxygen level dependent (BOLD) response from fMRI (Huppert et al., 2006; Kleinschmidt, 1996; Steinbrink et al., 2006; Strangman et al., 2002).

To date, researchers have not explored the use of simultaneous scalp EEG and fNIRS in determining the modulation of hemodynamics by spontaneous neural activity over a wide range frequencies and topographic regions of the human whole-head. The goal of this study was to fill this gap by examining the relationship between resting state EEG and the local hemodynamic response and, in particular, determining how EEG cross frequency coupling affects this relationship. We use the term whole-head to refer to the fact that we placed sensors at all standard 10-20 sites bilaterally covering the frontopolar, frontal, central, temporal, parietal, and occipital areas. The signals from EEG+fNIRS depend on neurovascular coupling, the processes through which neural activity affects local hemodynamic properties. Neurovascular coupling has been a topic of major interest due to its relationship with pathological brain physiology. There is evidence that neurovascular coupling is affected by aging, anesthesia, and diseases including depression, stroke, hypertension, Alzheimer's, epilepsy, subarachnoid hemorrhage, and traumatic brain injury (Attwell and Iadecola, 2002; Bari et al., 2012; D'Esposito et al., 2003; Girouard and Iadecola, 2006; Len and Neary, 2011; Lindgren et al., 1999; Malonek, 1997; Masamoto and Kanno, 2012). This study was intended to investigate the utility of human whole-head EEG+fNIRS in tracking neurovascular coupling in cortex.

METHODS

Subjects and Study Design

Eighteen healthy adult volunteers took part in this study (16 male; age mean 26 years (range 24-28 years)). None had a history of psychological illness or substance dependence. Subjects completed informed consent before the experiment and were compensated for their participation. The research was approved by Institutional Review Board at University of Houston. Each subject was seated in a comfortable chair in a silent room with lights dimmed and instructed to relax with eyes closed without exerting any mental effort or falling asleep. The resting state recording lasted 15 minutes. In order to investigate the gamma power modulation of Hb (HbO or HbR) we conducted a side study where 4 subjects were asked to briefly clench their jaw (~1 s) twice separated by 30 s. This was repeated 3 times in a recording that lasted 6 minutes.

Triplet Holder and Whole-Head Arrangement

Our multi-modal recording system has a basic module that consists of three components: a thin plastic holder, optodes, and electrodes (Figure 1). Determining the source-detector distance was critical for achieving the greatest possible sensing depth while maintaining sufficient signal quality. The instrument setup before a recording included an automated calibration stage where the optimum gain, or signal amplification, providing the best signal to noise ratio (based on the signal's coefficient of variation) for each source-detector pair was determined. Preliminary recordings were performed with source-detector distances in the range 20 mm - 40 mm. We observed that the best signal to noise ratios occurred with separations 30 mm or less, while greater separations frequently lead to problems in calibration and delays in the setup. In order to achieve the highest sensing depth with the quickest setup times, we therefore selected to work with a 30 mm source-detector separation. A thin plastic component was designed to hold the triplet of probes for the purpose of associating every EEG channel closely with a corresponding fNIRS channel. fNIRS optodes and EEG electrodes were in good contact with the scalp in order to ensure appropriate optical contact and low impedance. The holder was flexible in order to suit

the consistency and curvature of the scalp and provide a comfortable fit to the subject. The triplet holder was made rectangular for added geometrical stability and it was manufactured by a laser cutter. Nineteen passive Ag/AgCl EEG electrodes (Ladybird by G.Tec, Graz, Austria), 19 dual-wavelength LED emitters and 19 detectors were used for the whole-head arrangement. For added stability the triplet holders were mounted on an extended EEG cap (EasyCap 128, Brain Products GmbH, Germany). Activity was recorded over the whole-head with triplet holders placed according to the International 10-20 system (Fp1, Fp2, F7, F3, Fz, F4, F8, C3, Cz, C4, T7, T8, P7, P3, P4, P8, Pz, O1, O2) (Figure 2). The EEG reference and ground electrodes were located, respectively, at FCz and Fpz.

Data Acquisition

All data were simultaneously acquired with our EEG+fNIRS system. NIRScout extended dual-wavelength continuous wave system (NIRx Medical Technologies, New York) was used at a sample rate of 6.25 Hz for NIRS measurements. The two wavelengths were set at 760 and 850 nm. NIRStar software (NIRx) was used to check signal quality before starting each experiment and to acquire data. EEG signals were collected at 250 Hz sample rate using microEEG, a miniature (80 g), battery operated, wireless data acquisition system (Bio-Signal Group Inc., Brooklyn, New York). microEEG digitizes signals close to the electrode at 16 bits resolution and transmits them via Bluetooth to a nearby standard personal computer running Microsoft Windows. Both systems' sample rates were more than sufficient to collect the signal variations of interest for our subsequent analysis. The synchronization between EEG and NIRS was performed using the event triggers generated by Presentation software (Neurobehavioral Systems Inc.) during data acquisition.

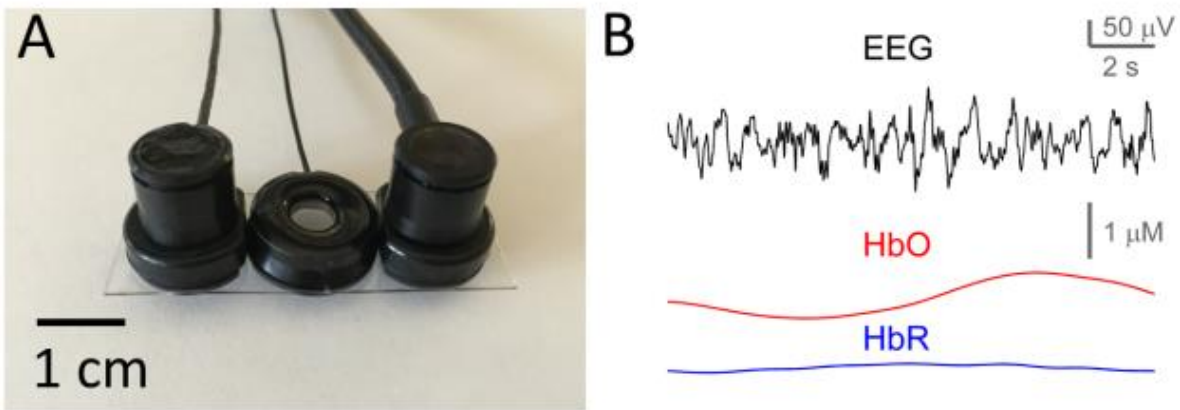


Figure 1 EEG+fNIRS recording module and the corresponding triple time series. **(A)** NIRS source detector (left-right) pair approximately 3 cm apart, flanking an EEG electrode (middle) held by the triplet holder. **(B)** Example of synchronized signals (EEG, HbO, HbR) measured from the sensors in a module.

Preprocessing and Validation

The signals were band-pass filtered (EEG: 0.5-80 Hz and NIRS: 0.01-0.5 Hz) with a sixth order Butterworth filter. The EEG was notch filtered at 60 Hz to eliminate power line noise. The EEG sample rate provided more than sufficient time resolution to capture the frequencies we expected to find in scalp EEG and the low-pass cut-off frequency for the EEG filter was set at 80 Hz in order to allow only components well below the Nyquist frequency (Van Drongelen, 2006). Experiments and modeling indicate that cortical contribution to the scalp EEG in the gamma frequency and beyond is small to negligible (Cosandier-Rimélé et al., 2012; Petroff et al., 2015). The low-pass cut-off for the NIRS filter was 0.5 Hz since we aimed to eliminate the heart-rate artifacts (~ 1 Hz) while capturing the underlying hemodynamics that change slowly on a timescale of several seconds. This low-pass cut-off frequency was not below the rates of breathing (0.2-0.4 Hz) or the Mayer waves (~ 0.1 Hz) hence these physiological signals were not filtered out (Scholkmann et al., 2014). This was due to the fact that they partially overlapped

with the time scale of the hemodynamic response which was being investigated. The effects of Mayer waves (which are part of the autocorrelation structure of the fNIRS signals and therefore influence the cross correlation between EEG power and fNIRS) were readily observable by their typical frequency and relatively large amplitude and therefore did not obscure our single subject results. In addition since the phases of the Mayer waves were randomly distributed among the subjects their effects were mitigated when the results were subject averaged. Furthermore there were no externally imposed time markers (such as stimuli or task performance) that could have driven EEG power and hemodynamics separately but in a coordinated fashion, and thereby created the cross correlations that we studied. Had we used low-pass cut-off frequency ≤ 0.5 Hz we would have removed features with timescales ≥ 2 s and not been able to detect the cortical hemodynamic responses that were of interest for this study. From the NIRS signals the concentration of oxy-hemoglobin and deoxy-hemoglobin were computed using the modified Beer-Lambert Law (MBL) (Delpy et al., 1988). The MBL describes an exponential attenuation of light between a source and a detector along a path whose effective length is a multiple of the source-detector separation. The effective path length is obtained by multiplying the source-detector separation by the Differential Path Length Factor (DPF) that is dependent on the wavelength of the light emitted by the source. We assumed that the only absorbers of light were HbO and HbR (Scholkmann et al., 2014). For 760 nm and 850 nm, we used the extinction coefficients, respectively, 1486.6 and 2526.4 for HbO and 3843.1 and 1798.6 for HbR, in units of $\text{cm}^{-1}\text{M}^{-1}$ while the corresponding DPF values were 7.25 and 6.38 (Jacques, 2013; Xu et al., 2014). The extinction coefficients of other chromophores such as water were an order of magnitude smaller than those of Hb and were ignored (Boas et al., 2001). For each channel the power spectrogram of the EEG was computed using a $\Delta W = 1.2$ s Hamming window with 50% overlap. The frequency resolution of the spectrograms were therefore $\Delta f = 1/\Delta W = 0.83$ Hz which was more than sufficient since we were interested in the coupling of the hemodynamics to the EEG power in bands wider than Δf . The EEG spectrograms and optical time series were

then resampled at a global rate of 2 Hz. We verified that changing the spectrogram time window size and the global resample rate within a wide range had negligible effect on our results. Calculations described in this paper used Matlab v.8.2.0.701 (The MathWorks, Inc., Natick, Massachusetts, United States), in particular the built-in functions *spectrogram*, *xcorr*, *conv*, and *kstest2*. We used the referential montage for EEG in this study. The processed signals were visually inspected for the effects of muscle and motion, eye movements, and other artifacts. Suspected sleep patterns in the EEG (also based on self-reporting) were also considered as artifacts. The recordings that were contaminated in excess of 10% by artifact were excluded as a whole. Thus 12 of the 18 subjects who were recorded were included for further analysis. In the included studies any brief segment containing artifact in either time series were manually removed from both EEG and fNIRS.



Figure 2 Triplet holders distributed at 10-20 positions held together by a cap. 19 locations arranged according to the International 10-20 System were selected over the whole head.

Analysis

Cross correlation. The EEG power at the frequency f at time t was denoted $p(f,t)$. The hemoglobin concentration changes were denoted $h_i(t)$ with $i=1$ and 2 corresponding to HbO and HbR, respectively. We centered and normalized each subject's $p(f,t)$ and $h_i(t)$ in order to eliminate the effects of their amplitudes and focus only on the degree of the coupling of their fluctuations. We computed the delayed correlation of EEG power with Hb as

$$c_i(f,\tau) = \langle p(f,t)h_i(t+\tau) \rangle, \quad (1)$$

where $\langle \cdot \rangle$ represented time averaging over the duration of an experiment. The EEG frequency band powers, $p^{(k)}(t)$, used in clinical practice were computed by averaging $p(f,t)$ over ranges of frequency. For $k=\delta, \theta, \alpha, \beta$, and γ we used the ranges 0–4 Hz, 4–8 Hz, 8–16 Hz, 16–32 Hz, and 32–80 Hz, respectively. The corresponding delayed correlations, $c_i^{(k)}(\tau)$, were found by substituting $p^{(k)}(t)$ for $p(f,t)$ in Equation (1).

Statistical significance. In order to assess the significance of the estimates of the correlations from our experiments we compared them with the baseline variability of the correlation that was obtained as follows. In RS data we did not expect fluctuations of neural activity in one recording to drive the hemodynamics in a different recording. Such correlations of pairs of distinct recordings could therefore be used to provide a noise level indicator for our correlation values. We calculated correlations between neural activity and hemodynamics by using pairs of EEG and Hb data taken from pairs of distinct recordings. For a set of $N=12$ recordings, there were $N(N-1)=132$ such distinct pairs, which helped create a large reference set of baseline data. For each EEG power frequency, we segmented correlation time delays into $\Delta\tau=4$ s intervals and assessed the significance of the values of $c_i^{(k)}(\tau)$ at the center of each interval. The size of $\Delta\tau$ was selected to be sufficiently small to track the characteristic changes in $c_i^{(k)}(\tau)$ while

remaining large enough to avoid an excessive number of comparisons and maintain clarity. We formulated the null hypothesis that the distribution of the values of $c_i^{(k)}(\tau)$ for the N recordings was the same as that of the values in the reference set. The distribution of values in the reference set was highly non-Gaussian (kurtosis = 3.76) and we chose the relatively conservative Kolmogorov-Smirnov test to evaluate null hypothesis. The significance level was Bonferroni corrected to account for the multiple comparisons to the p-value = 0.05/15 = 0.0033 since there were 15 intervals within the maximum time delay range of 60 s.

Extraction of the hemodynamic response function. The delayed correlation was a helpful manifestation of the time-frequency dependent neurovascular coupling. However it was an unresolved admixture of underlying responses to various frequencies. Multi-modal data allowed us to go further by applying system identification techniques. We used EEG power and Hb time series in a correlation analysis based on a model of neurovascular coupling (Biessmann et al., 2011; Dahne et al., 2013). In the model the neurally modulated part of hemodynamics was the convolution of EEG power with $R_i(f, \tau)$, the hemodynamic response function (HRF):

$$h_i(t) = \sum_f \sum_{\tau} R_i(f, \tau) p(f, t - \tau). \quad (2)$$

HRF expressed the delayed response to the EEG rhythm at frequency f . We substituted (2) into (1) to obtain:

$$c_i(f, \tau) = \sum_{f'} \sum_{\tau'} A(f, \tau, f', \tau') R_i(f', \tau') \quad (3)$$

where the EEG power autocorrelation was $A(f, \tau, f', \tau') = \langle p(f, t)p(f', t + \tau - \tau') \rangle$. This indicated that the autocorrelation structure of EEG power had to be examined in order to extricate HRF from the correlations. Formally, the HRF could be solved for by inverting Equation (3). Such a direct approach was not advisable due to potential numerical instability and other

problems related to noise amplification (Chatfield, 2004). We sought to develop a relatively straightforward nonparametric time-domain approach. We assumed that the autocorrelation was separable in the frequency and time variables and, in addition, its time dependence was described as a delta function:

$$A(f, \tau, f', \tau') = \rho(f, f') \delta_{\tau\tau'}. \quad (4)$$

Here $\rho(f, f')$ was the zero-lag autocorrelation and $\delta_{\tau\tau'} = 1$ if $\tau = \tau'$ and $\delta_{\tau\tau'} = 0$ otherwise. This approximation was supported by our Results (Figure 7) and it led to $c_i(f, \tau) = \sum_{f'} \rho(f, f') R_i(f', \tau)$. The HRF was then found as

$$R_i(f, \tau) = \sum_{f'} \rho^{-1}(f, f') c_i(f', \tau). \quad (5)$$

We explored the validity of this method by applying it to part of our data.

Modeling of the hemodynamic response function. We also investigated the extent to which the HRF could be parametrically quantified. For this purpose a difference-of-Gammas model was utilized. Since coupling in the alpha range was particularly salient we chose to focus on the response to the alpha rhythm:

$$R_i^{(\alpha)}(\tau) = \Gamma_{i,1}(\tau) - r_i \Gamma_{i,2}(\tau) \quad (6)$$

where each gamma function:

$$\begin{aligned} \Gamma_{i,k}(\tau) &= \left(\frac{\tau}{t_{ik}} \right)^{a_{ik}} \exp\left(-\frac{\tau - t_{ik}}{b_{ik}} \right) \\ a_{ik} &= C(t_{ik} / w_{ik})^2 \\ b_{ik} &= w_{ik}^2 / (Ct_{ik}). \end{aligned} \quad (7)$$

The model was based on the FMRISat algorithms (Proulx et al., 2014; Worsley et al., 2002). The constant was $C = 8 \log 2$. This model initially rises, peaking at time t_{i1} , then decreases until a trough is reached at time t_{i2} , and finally decays to zero. The full widths at half magnitude of

corresponding peaks were determined by the parameters w_{i1} and w_{i2} . The parameter r_i set the absolute magnitude of the second peak relative to that of the first. The characteristic rise and fall time scales of the gamma functions were determined by the variables a_{ik} and b_{ik} . The two models for HbO and HbR therefore collectively contained a total of 10 free parameters: t_{ik} , w_{ik} and r_i , with $k = 1, 2$ and $i = 1$ (HbO) and $i = 2$ (HbR). Each subject's HbO and HbR were simulated by convolving the alpha band power with $R_i^{(\alpha)}(\tau)$ given by Equation (6). From the resulting time series delayed correlations were computed and compared with the experimentally observed HRF. The parameter values were determined by grid search that minimized the mean square difference between the simulated and the observed correlations.

RESULTS

An example of the preprocessed data from one resting state experiment is shown in Figure 3. The figure shows a 2 minute segment selected based on its ability to illustrate several features frequently encountered. Noteworthy are the dominant posterior alpha rhythm at approximately 10 Hz particularly strong in the occipital and parietal channels but visible almost globally. The figure also illustrates the spontaneous fluctuations in the amplitude of the alpha oscillation. Close examination of the spectrogram in F7 reveals higher power in narrow ranges at multiples of the NIRS sample rate 6.25 Hz. This is an example of an artifact created by a NIRS source cable when it is close to an EEG lead and eliminated by rearrangement of the cables. Another noteworthy feature in Figure 3 is that the HbO (red curve) appeared to surge in the frontal and temporal channels F7, F8, T3, and T4 toward the end of the time segment shown, returning to baseline after about 20 s. The HbR (blue) during the same period underwent a dip smaller in amplitude and delayed with respect to the HbO. We verified in separate experiments, described

further below, that this pattern is activated when the subject clenches her jaw contracting the temporalis muscle located directly under those channels.

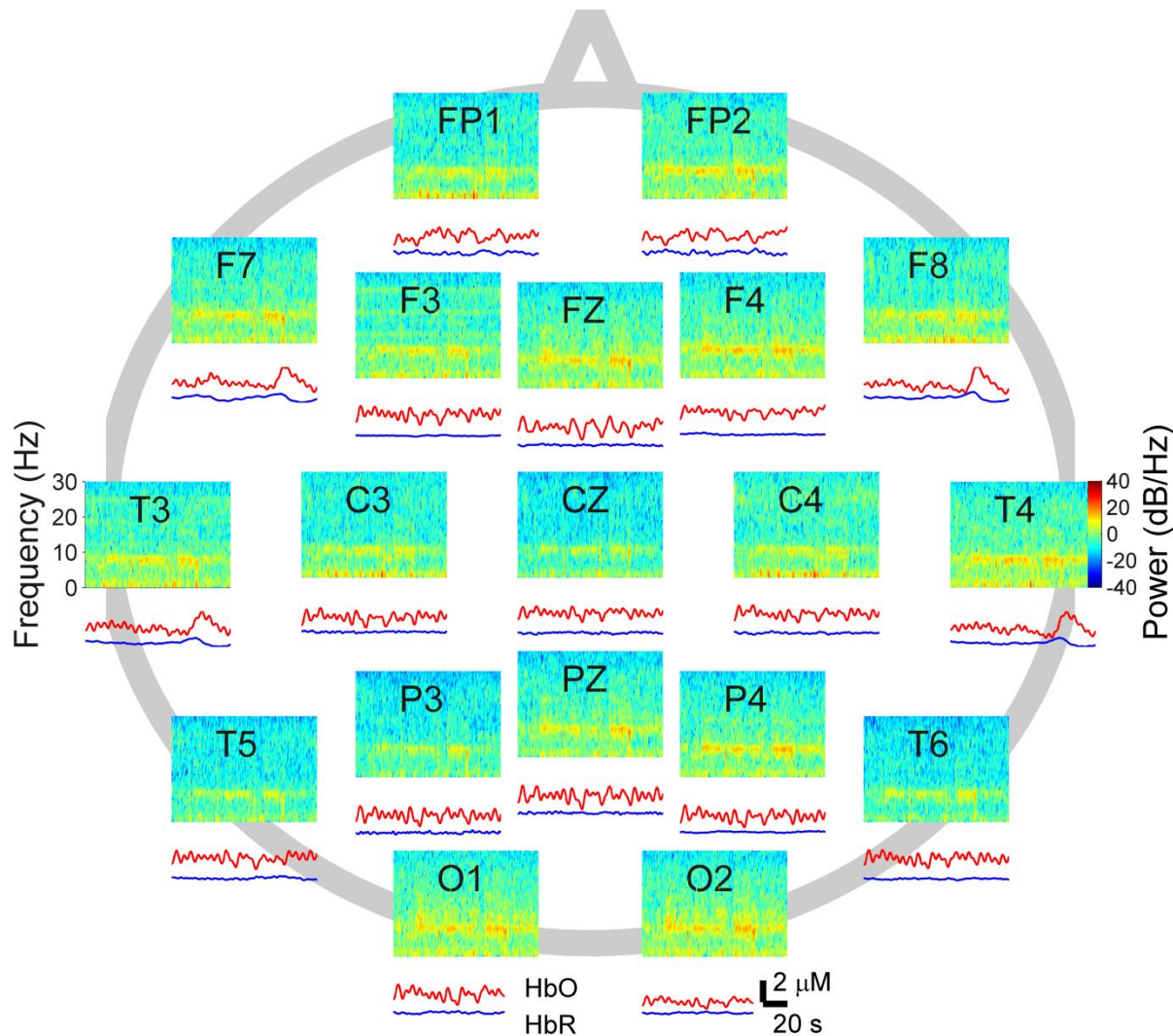


Figure 3 Example of EEG and fNIRS data recorded simultaneously from the whole head. At each of the 10-20 locations are shown an EEG spectrogram and the corresponding HbO (red) and HbR (blue) time series.

Figure 4 displays the delayed correlations (for HbO only) for 4 of the total of 12 experiments included in the study. Experiment numbers are indicated at the top left of each figure. The subset in Figure 4 was selected due to its ability to exemplify most of the features that were

observed in all of our experiments. Some of the inter-subject variability observed in this figure was as follows. In experiment 1 the delayed negative correlation in the alpha band in posterior areas was accompanied by another peak with the opposite sign at the nearby theta band with a similar delay. In experiment 2, the strongest negative correlation occurred in the beta band. In experiment 3, the negative correlation appeared to be distributed equally in the alpha and beta bands. Despite such inter-subject variability, however, the most salient feature shared by most subjects was a negative correlation between the EEG power, particularly in the alpha and beta frequency ranges, and the HbO concentration changes with a delay at approximately 8 s. This appeared most strongly in the parietal and occipital areas but was also approximately replicated in the frontopolar regions. The strong positive correlation with gamma power observed in some subjects (e.g. experiment 1 and others not included in Figure 4) in channels T3, T4, F7, F8 was due to contamination from the scalp muscles. Figure 4 contained an apparently anticipatory hemodynamic signal in subjects 2 and 4, while another experiment (not shown) contained a small positive correlation between HbO and EEG alpha at about 8 s which was the opposite of the group average. In many experiments there was, in addition, a pattern of zero-lag correlation distributed across higher frequencies (such as T3 in Experiment 1 in Figure 4). This was attributable to a motion artifact introduced by the contraction of temporalis muscle that simultaneously affects the EEG and NIRS probes. We verified the muscle origin of these features in a further experiment (Figure 13). The correlations for HbR (not shown) for each subject were similar to the corresponding HbO correlations but with an opposite sign, and a longer time delay.

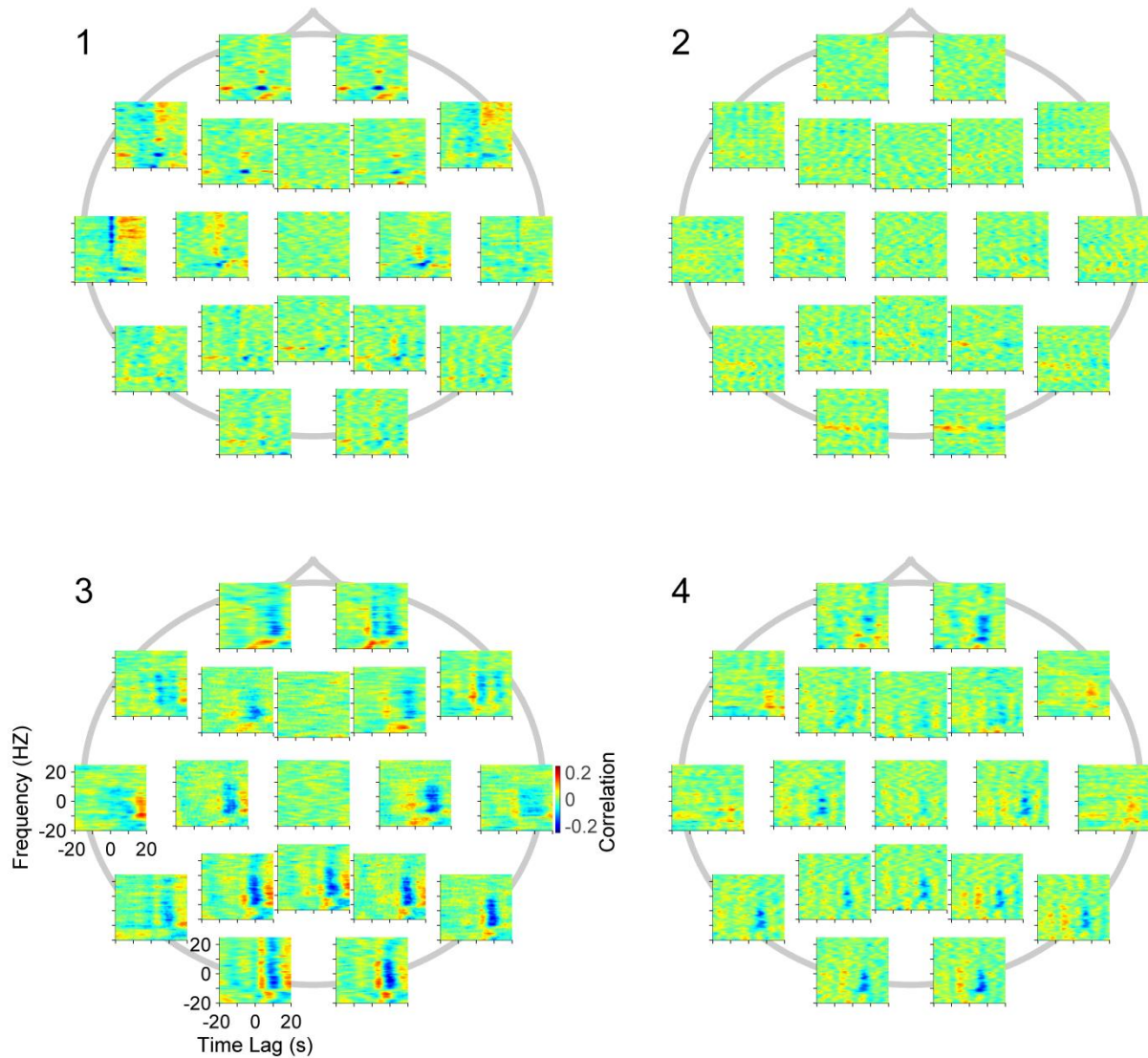


Figure 4 The position and frequency dependent delayed correlations between EEG power and HbO for four representative subjects.

We visualized the EEG power-Hb correlations by averaging over subjects and within three distinct topographic regions. We used the EEG power lumped over each frequency band used in clinical practice. The regions were 1) Frontopolar (FP1, FP2); 2) Inferior electrodes (F7, F8, T3, T4); and 3) Parietal and occipital (P3, Pz, P4, O1, O2) channels. Figure 5 shows the results for regions 1-3 as rows 1-3 with the columns corresponding to distinct frequency bands. The thick curve is the subject and region average while the shaded region represents one standard

deviation around the mean for the group of experiments. An asterix indicated that the amplitude of the correlation is statistically significant in accordance with a Kolmogorov-Smirnov test described in Methods. The vertical dotted lines mark the location of zero-lag. The figure indicates that the strongest coupling occurred in the alpha and beta bands in the occipital and parietal regions and at the inferior electrode sites. The latter was of muscular origin and was frequently accompanied by a sharp feature at zero-lag due to motion artifact. The corresponding delayed correlations for HbR shown in Figure 6 had similar features but the peaks were negative, wider, and delayed by several seconds. This was consistent with the time course of HbR relative to HbO generally observable in their time series, an example of which was provided in Figure 3.

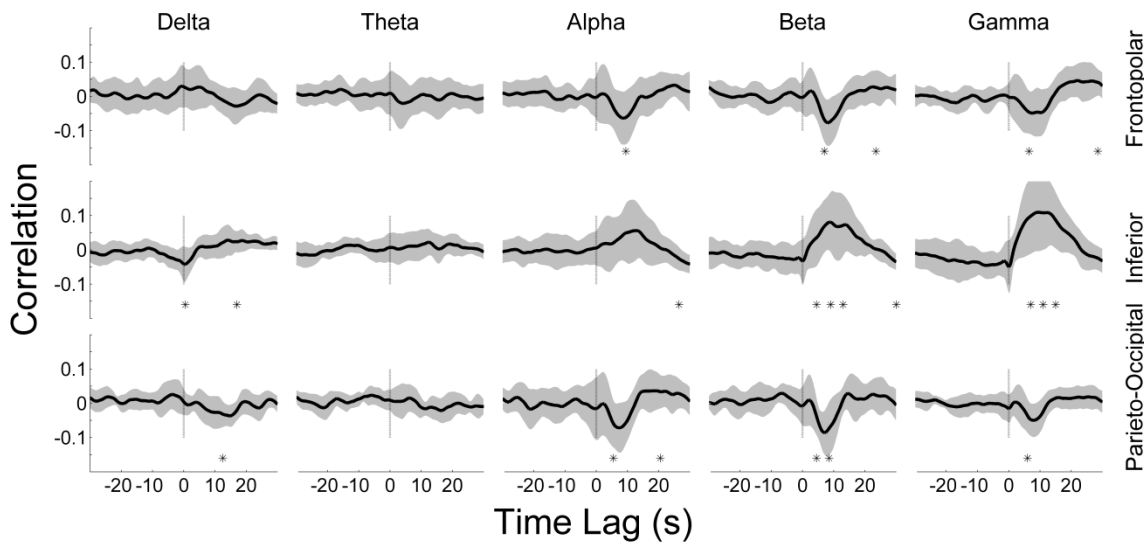


Figure 5 EEG power-HbO correlations at the standard EEG frequency bands delta (0-4 Hz), theta (4-8 Hz), alpha (8-16 Hz), beta (16-32 Hz), and gamma (32-80 Hz) shown in columns. The top row is the average of the frontopolar (FP1, FP2) channels; the middle row inferior electrode sites (F7, F8, T3, T4); and the bottom row parietal and occipital channels (P3, Pz, P4, O1, O2). An asterix indicates $p\text{-value} < 0.0033$ for the corresponding 4 s segment of the result. The vertical dashed line shows the position of zero time lag. The thick black curve is the mean and the shaded region is the standard deviation of the distribution over subjects.

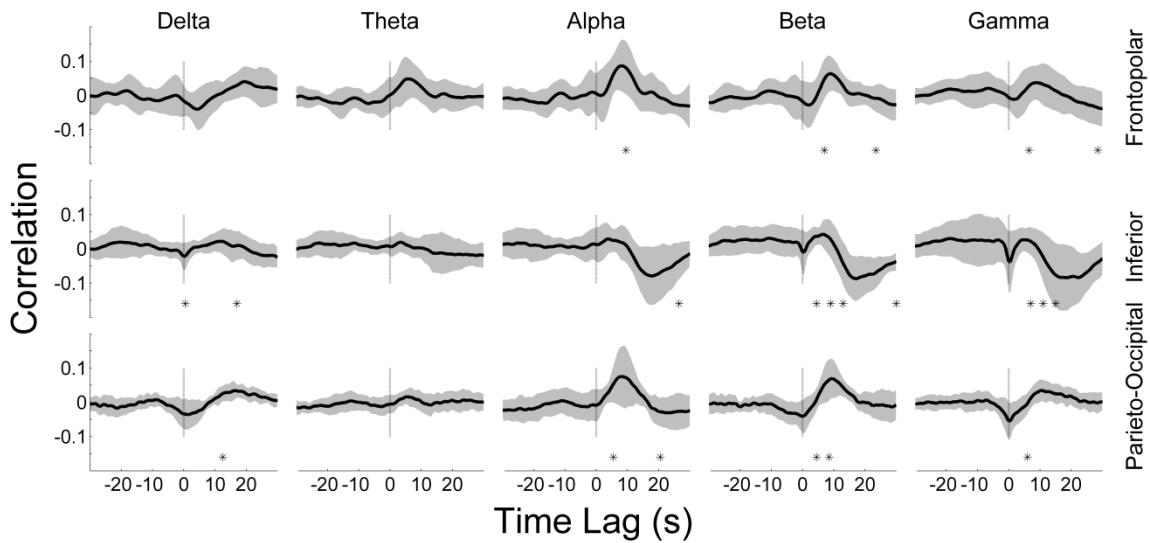


Figure 6 Same calculations described in Figure 5 with HbO replaced by HbR.

We further investigated the implications of the foregoing results for the frequency resolved HRF. Equation (5) indicated that the HRF could be elicited from the delayed correlations by using the autocorrelation of EEG power, $A(f, \tau, f', \tau')$. We therefore began by examining the frequency and delay dependence of A . As shown by the middle column in Figure 7 the delay dependence of A was highly peaked at zero delay and hence supported the assumption made in Equation (4). Figure 7E indicated that the autocorrelation at 10 Hz decayed more slowly with delay than at the other frequencies shown. Overall, the autocorrelation quickly decayed with increasing delay and vanished after about 2 s. However this deviation from a true delta function was not expected to affect our calculation of HRF except for a small temporal broadening of the result.

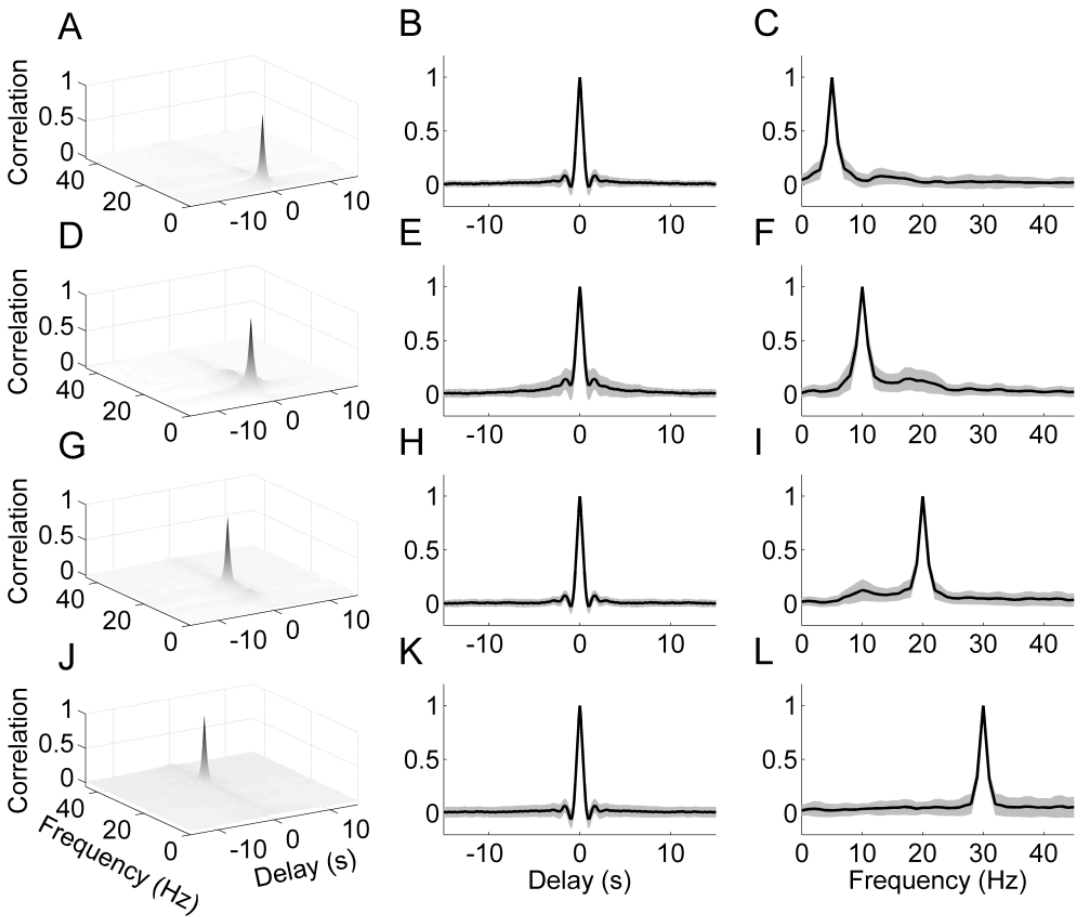


Figure 7 The autocorrelation of EEG power as a function of frequency and delay. In the middle and right columns the black curves represent the average and the shaded region represents one standard deviation from the average found from all channels and subjects. The top row is for $f = 5$ Hz. **(A)** The autocorrelation as a function of both the delay ($\tau - \tau'$) and the frequency f' ; **(B)** as a function of the delay ($\tau - \tau'$) at a fixed frequency $f' = 5$ Hz; and **(C)** as a function of f' at a fixed delay ($\tau = \tau'$). Rows 2-4, respectively, show corresponding results for $f' = 10$ Hz **(D-F)**; $f' = 20$ Hz **(G-I)**; and $f' = 30$ Hz **(J-L)**.

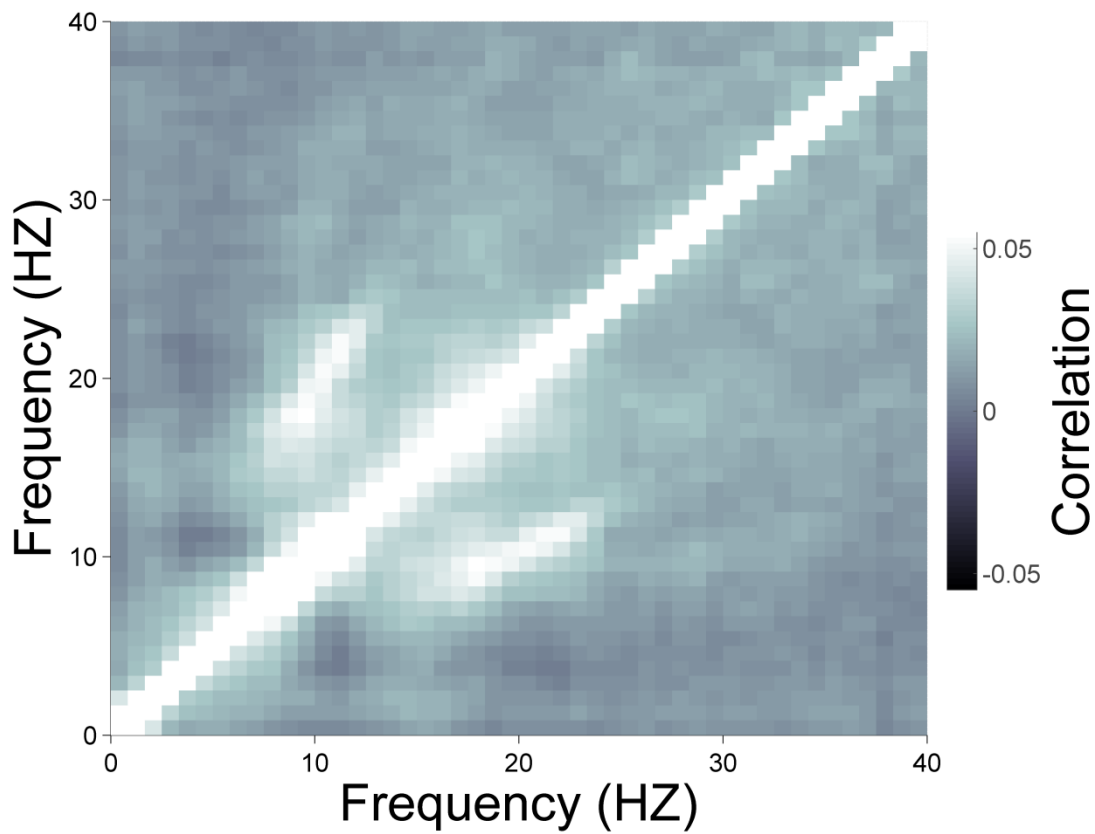


Figure 8 EEG power zero-lag autocorrelation averaged over subjects

Figure 7F and G show that EEG power at 10 Hz was coupled with the power at 20 Hz. For example Figure 7F contains a bump near 20 Hz. Similarly Figure 7I contains a bump near 10 Hz. These results indicated that the correlation of EEG power with Hb would be a mixture of the effects of the alpha and beta band activities. Figure 7C also showed that power at 5 Hz was coupling weakly with power at ~15Hz. By contrast gamma range power at 30 Hz did not show evidence of coupling with other frequencies (Figure 7L). The values shown in Figure 7 were subject averages.

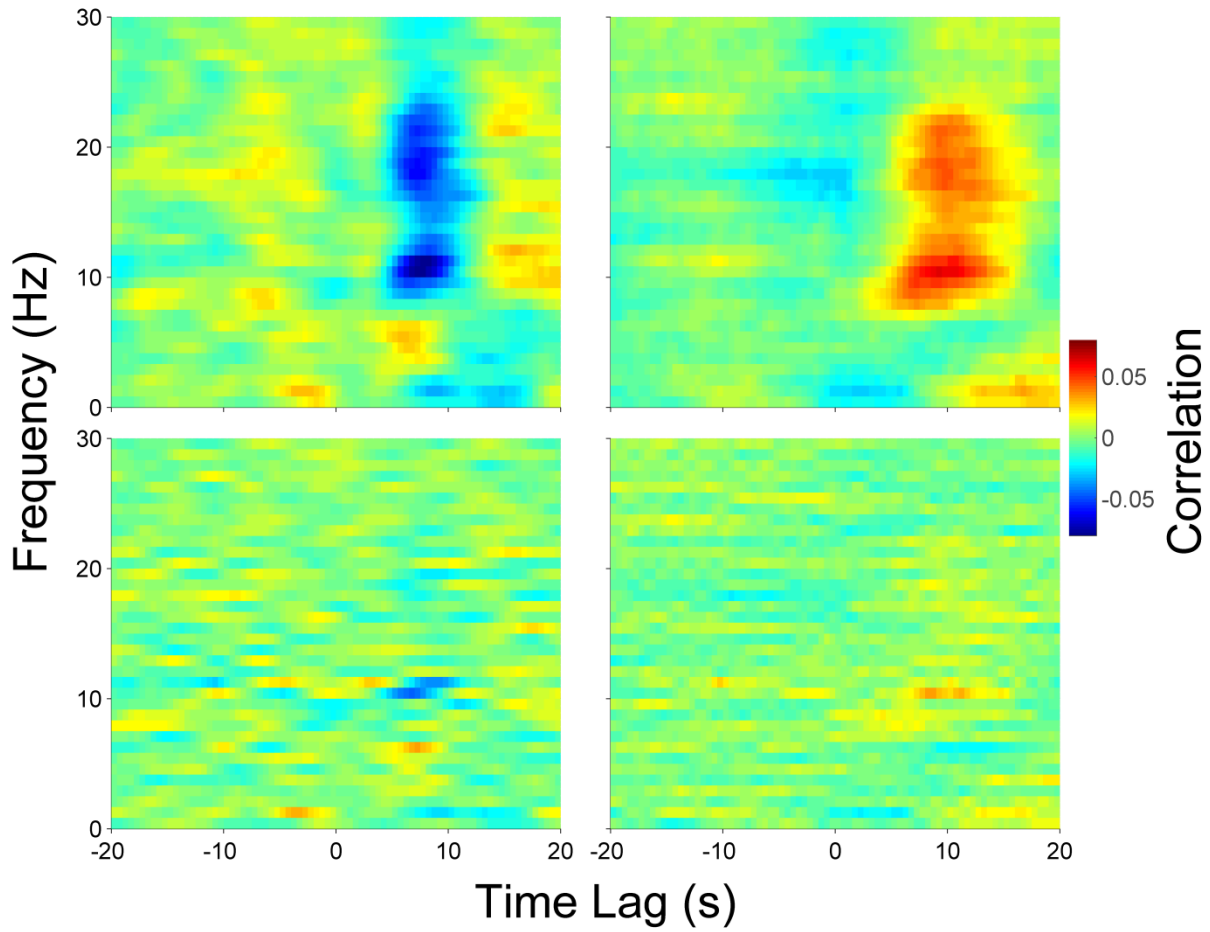


Figure 9 EEG power-Hb correlation for **(A)** HbO and **(B)** HbR averaged over subjects and over the parietal and occipital channels. The hemodynamic response function for **(C)** HbO and **(D)** HbR calculated from the correlation using Equation (5).

In order to closely examine the zero-lag autocorrelation of EEG power we plotted subject averaged $A(f, 0, f', 0)$ as a function of the two frequencies f and f' in Figure 8. The diagonal elements in Figure 8 had the value 1 while most of the other values were nearly zero with some specific exceptions. Firstly, the modest broadening of the lightly colored diagonal at ~ 10 Hz and ~ 18 Hz were indicative of stronger coupling of frequencies within the alpha and beta bands. More interestingly the power at ~ 10 Hz was strongly coupled with power at nearly double the

frequency (lightly colored bars symmetrically situated away from the diagonal). In addition the power at ~5 Hz was inversely correlated with the power in the alpha and beta ranges, as shown by the darker patches vertically and horizontally extending along the level of 5 Hz. The obvious alpha-beta coupling in Figure 8 further strengthened the expectation, based on Equation (3), that the values of $c_i^{(\alpha)}(\tau)$ and $c_i^{(\beta)}(\tau)$ would be closely related.

We investigated this relationship and the ability of Equation (5) to resolve the HRFs at distinct frequencies. Since the EEG power-Hb coupling appeared particularly strong in the parietal and occipital regions (Figure 4) we focused on the correlations averaged over these regions. Figure 9 strikingly demonstrated the alpha and beta range coupling of EEG power with hemodynamics. Figure 9A indicated that the EEG power-HbO correlations contained strong negative peaks centered at approximately $\tau=8$ s in the alpha and beta frequency ranges. In addition there appeared to be a weaker positive correlation at the same delay in the theta range (not statistically significant; also refer to Figure 5).

These relationships appeared to replicate the coupling among the EEG bands shown in Figure 8. There were temporally broader, positive peaks in the alpha and beta ranges of the EEG power-HbR correlation (Figure 9B) that occurred at approximately $\tau=10$ s. The absolute magnitudes of the peaks and the subsequent rebounds were slightly greater in the alpha range than in the beta. By contrast the HRFs computed by using Equation (5) and the correlation data in Figure 9A and the autocorrelations in Figure 8 suggested that the 8 s peaks in the HRF were driven solely by alpha-hemodynamics coupling (Figure 9C and D). Figure 10 compares HRFs with the correlations that they were derived from. The figure shows that the apparent coupling in the unresolved correlation at frequencies other than ~10 Hz is drastically lower in the HRF.

Figure 10 also suggests that in the theta range the HRF peak may be stronger than the correlation peak. The HRFs shown were averages over all subjects of the HRFs computed individually with subject specific data.

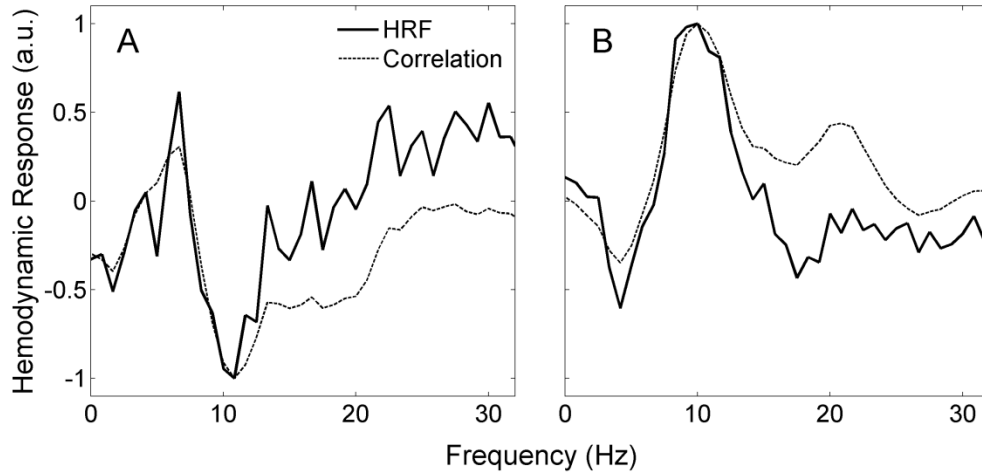


Figure 10 Hemodynamic response function (solid curve) and the correlation (dotted) as a function of the EEG power frequency averaged over time lags from -20 s to 20 s for (A) HbO and (B) HbR. The curves were smoothed by a sliding 2 Hz window and rescaled in order to have absolute value of their maxima equal to unity.

In order to pursue the alpha-hemodynamics coupling further, we calculated a simulated Hb signal for each channel and for each subject by convolving the alpha power with a HRF that was modeled as a difference-of-Gammas function (Equation (6)). From the simulated hemodynamics we calculated the delayed correlations for HbO and HbR and fitted the channel and subject averaged correlations to those that were experimentally obtained. We obtained the parameter values for the HRF models from a grid search that minimized the mean squared error between the simulated and experimental result. The optimum values were, for HbO, $t_{11} = 7.8$, $w_{11} = 5.95$, $t_{12} = 12.16$, $w_{12} = 16.35$, and $r_1 = 0.37$, and for HbR, $t_{21} = 8.5$, $w_{21} = 7.3$, $t_{22} = 21.4$, $w_{22} = 20.31$, and $r_2 = 0.331$. The model based and experimental correlations are shown in

Figure 11. The thick red and blue curves represent the correlations based on convolving, for each parietal and occipital channel and subject, the alpha power with the model HRFs for HbO and HbR, respectively. The thin dark red and dark blue curves are the experimental channel and subject averaged correlations. Figure 12 displays an example of the alpha power time series (A) and simulated time series for HbO (B) and HbR (C) obtained by convolving alpha power with the model HRF. The data were chosen from a representative subject and time segment in order to illustrate the fact that simulated Hb time series driven only by EEG alpha power agree well with actual Hb time series (Pearson correlations for the HbO and HbR segment shown were 0.49 and 0.70, respectively).

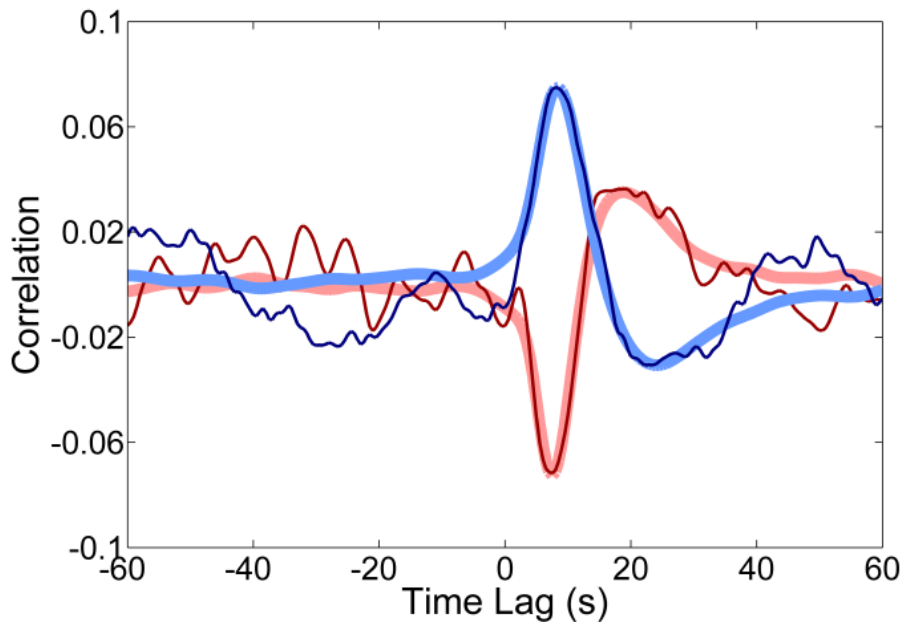


Figure 11 Hemodynamic response functions in the alpha range from simulated (thick curves) and experimental (thin curves) data. Simulated Hb were obtained by convolving alpha power with the modeled response (Equation (6)) then used to compute delayed correlation of the HbO (thick red curve) and HbR (thick blue) to alpha power. Experimental response functions are shown for HbO (thin dark red) and HbR (thin dark blue). Results were averaged over the parietal and occipital channels and all subjects.

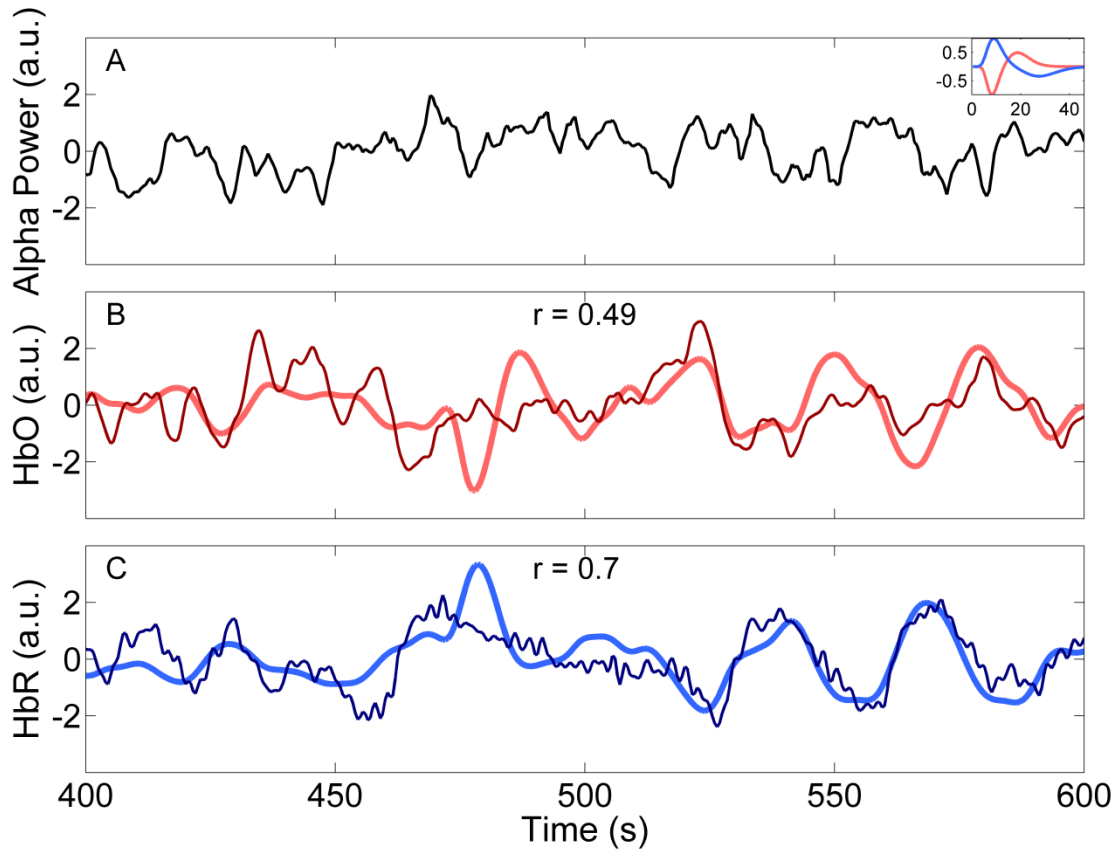


Figure 12 The EEG alpha power (A) and simulated HbO (B, thick red curve) and HbR (C, thick blue) compared with the actual HbO (B, thin dark red curve) and HbR (C, thin dark blue) for a representative time segment and subject. Pearson correlations between the simulated and actual result for the displayed time segment are shown next to the corresponding data. The inset at the top right shows the hemodynamic response curves (for HbO (red) and HbR (blue)) used in the simulation. Data were centered and normalized to unit standard deviation.

Some subjects (e.g Experiment 1 in Figure 4) showed evidence of EEG power-Hb coupling in the gamma range. We investigated the origin of such patterns in a separate set of experiments. Relatively large Hb fluctuations following EEG gamma activity had been occasionally found in our RS experiments. The results of the side study indicated that the EEG gamma power surge

was of muscular origin and almost invariably lead to subsequent hemodynamic excursions. Time series data from a representative experiment are shown in Figure 13. The EEG spectrograms in the figure at most 10-20 sites showed salient high frequency activity at $t = 10$ s and 40 s. These time points also coincided, only at the inferior electrode sites, with a sharp dip in the Hb signals. This was due to the brief change in the coupling of the optodes to the scalp caused by the contraction of the temporalis muscles located under T3, T4, F7, and F8. These time points also coincided with the onset of a substantial surge in HbO which peaked about 10 s later and returned to baseline after 30 s. The HbR time-course, after a small initial rise, followed a pattern that was a mirror image of the behavior of HbO, but with smaller amplitude and a relative delay of 2 s.

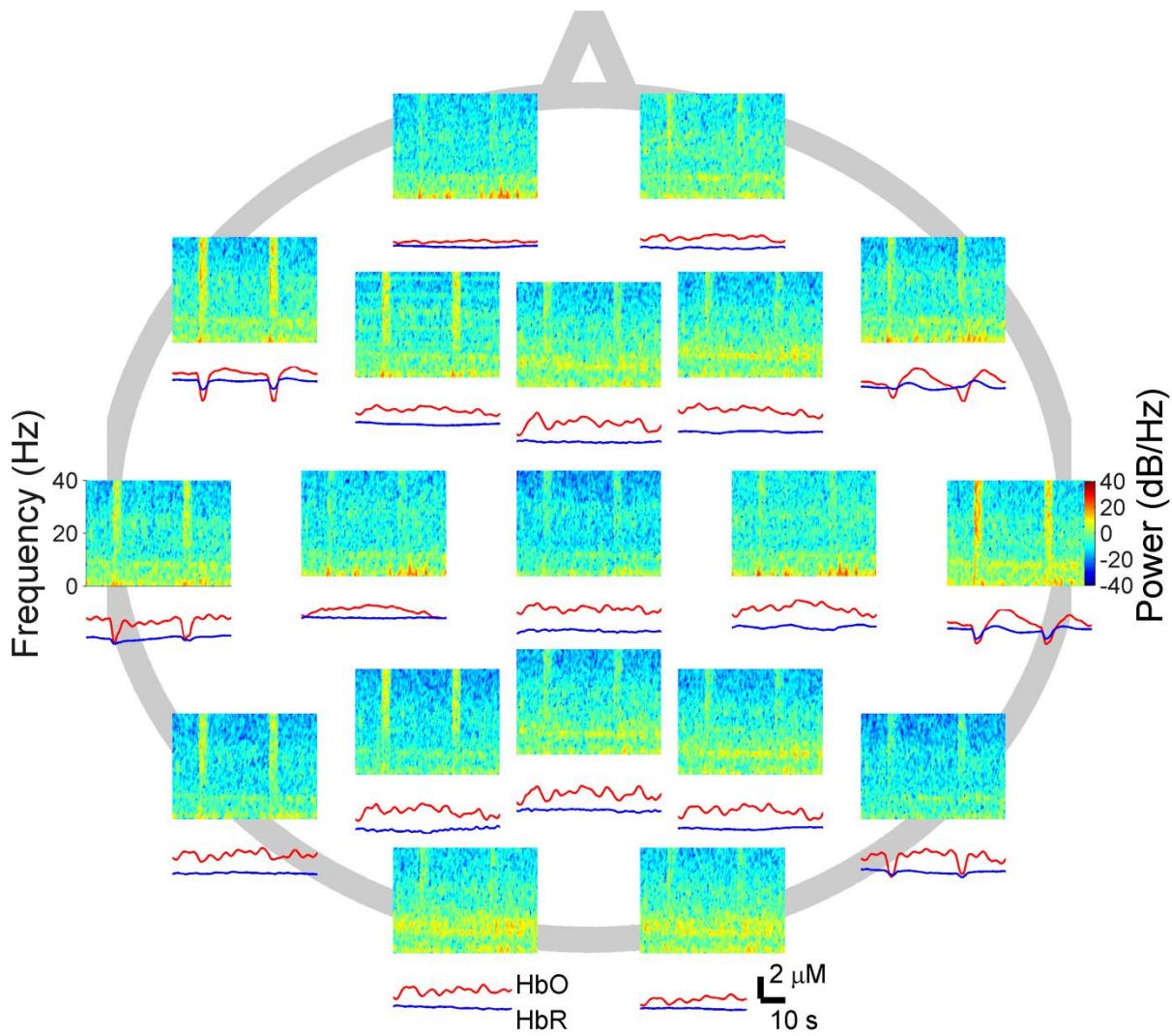


Figure 13 Example of EEG and fNIRS data recorded simultaneously from the whole head in a jaw-clenching experiment. At each of the 10-20 locations are shown an EEG spectrogram and the corresponding HbO (red) and HbR (blue) time series. The vertical axes of the spectrograms indicate the frequency and their color code indicates power units of dB/Hz.

DISCUSSION

To our knowledge this is the first study that (1) uses fNIRS channels co-located with all EEG electrodes at the standard 10-20 sites, and (2) closely examines the influence of EEG cross frequency correlations on the relationships of hemodynamics with EEG power. We have confirmed that significant information about neurovascular coupling is available from scalp EEG+fNIRS. Our results have highlighted the feasibility of noninvasive, whole-head EEG+fNIRS in studying the neural modulation of hemodynamics over the range of EEG rhythms familiar in clinical practice. Our results also showed the importance of disentangling the contribution of distinct rhythms to the correlation between EEG and fNIRS signals. For this purpose we proposed a nonparametric approach and demonstrated its utility. The results were further corroborated by data simulations using a model of the response to alpha power, which showed a close fit between the observed and predicted hemodynamic responses. Finally we compared the artifacts from jaw clenching in EEG and fNIRS.

The alpha modulation of brain hemodynamics was known from numerous previous studies (De Munck et al., 2007; Feige, 2005; Goldman et al., 2002; Goncalves et al., 2006; Laufs et al., 2003; Moosmann et al., 2003; Wu et al., 2010). In Moosmann et al. (2003) the EEG was measured from human subjects in the resting state simultaneously with fNIRS. They convolved the EEG alpha power with a canonical HRF model to obtain a reference alpha signal. They found that the correlation with the reference signal had a positive correlation with HbR in the occipital cortex. The correlation was highest when the HRF was configured to peak at 8 s. They concluded that enhanced alpha activity in occipital cortex was associated with metabolic deactivation. The peak frequency of the alpha wave has intra-subject consistency while it may differ between individuals. (Koch et al., 2008) studied the predictive value of individual alpha frequency (IAF) for the neuronal and vascular responses to visual stimulus. They also recorded

EEG and fNIRS in the resting state and found that alpha power inversely related to the IAF. In addition high IAF predicted low oxygenation response. (De Munck et al., 2007) used simultaneous EEG and fMRI to obtain an alpha band hemodynamic response that contained a peak latency at ~8 s in the occipital areas during eyes closed resting state.

The modulation of hemodynamics by EEG power investigated in previous studies was not limited to the alpha band. In (Roche-Labarbe et al., 2008) simultaneous EEG and fNIRS were recorded from neonates in quiet sleep. They investigated the hemodynamic response to brief spontaneous bursts of delta and theta activity. The bursts were found to be coupled to stereotyped hemodynamic responses involving an initial (3-4 s) decrease in HbO sometimes starting a few seconds before a burst. The decrease was followed by a positive peak at about 10 s and subsequent return to baseline. They also found that response in neonates in neurological distress systematically deviated from this pattern. Ritter et al., (2009) used simultaneous EEG and fMRI during a motor task and found that BOLD signal inversely correlated with the Rolandic beta rhythm in the precentral cortex. In another study (Mantini et al., 2007) used simultaneous EEG and fMRI in the resting state to investigate the EEG power correlates of the default mode networks identified through the functional connectivity of the BOLD signal. Their results showed that each network was differentially associated with variations of the delta, theta, alpha, beta, and gamma oscillations.

The characteristic hemodynamic time delays reported in these studies are consistent with our findings. The duration associated with hemodynamic response to stimulation, on the other hand, was reported (e.g. Logothetis and Wandell, 2004; Ou et al., 2009) to be briefer than that to changes in the alpha rhythm. De Munck et al. (2007) and Goncalves et al. (2006) found that a minority of their subjects had delayed alpha hemodynamic responses whose sign was reversed relative to the group average. Similarly, one of our 12 subjects showed a small positive

correlation between HbO and EEG alpha at about 8 s which had the opposite sign as that of the group average. One possible explanation for such variability is intersubject differences in hemodynamics. Another possibility is that hemodynamic response is non-stationary and the data we have collected were confounded by unknown state changes in RS. For example briefly falling into light sleep during RS is not uncommon and may have escaped the artifact removal stage.

Our results indicate that RS transient increases in neuronal synchronization in the alpha or beta frequencies (as indicated by a rise in EEG power in these bands) are typically followed by a decline in the oxygenated hemoglobin concentration. HbO is closely related to local cerebral blood flow (CBF), naturally leading to the conclusion that higher power in these bands correlates with lower metabolic demand. For this reason they have been referred to as "idle rhythms" although the function of these oscillations is not clear (Pfurtscheller et al., 1996). A possible mechanism for this has to do the fact that the transition to synchronization by a neuronal population may come about through diverse paths including changes in input, synaptic gain, and axonal delay (Sirovich et al., 2006). One such transition involves a *decrease* in the input to a population. Assuming that the synchronization in question follows this path (supported by the fact that alpha appears when the eyes are closed) then it would naturally be accompanied by a decrease in metabolic demand. Synaptic activity is believed to dominate metabolic demand (Buzsáki et al., 2012). Hence although the generation of the rhythm requires energy the net effect of increase in its power may well be a metabolic decrease followed by lower local CBF.

Possible anticipatory hemodynamic signal in a small subset of our subjects (Subjects 2 and 4 in Figure 4) was generally consistent with the presence of such patterns in animal study results (Sirotin and Das, 2009) and neonates (Roche-Labarbe et al., 2008). The appearance of seemingly anticipatory hemodynamics may be due to prior neural activity that is not picked up

by EEG. If this proves to be the case then it may be utilized in detecting patterns missed by scalp EEG.

Simultaneous intracranial electrocorticography and fMRI have indicated that a tight relationship exists between BOLD signal and broadband gamma in humans (Mukamel et al., 2005; Nir et al., 2007) and animals (Logothetis et al., 2001; Niessing et al., 2005). In our study the delayed negative correlation of EEG alpha and beta power with HbO was topographically widely distributed but absent at the inferior electrode sites where it was replaced the gamma modulation of Hb due to scalp muscle. In order to investigate if the muscle oxygenation was masking an underlying pattern we repeated the calculations in Figure 5 and Figure 6 using only the 3 subjects who by inspection had not shown gamma correlations. The results (not shown) contained no significant modulation of hemodynamics by gamma in any region.

We believe one of the main limitations of our study was that the spatial resolution of EEG was low and that the local neuronal input to the hemodynamics was not well resolved. This may account for the observed lack of significant associations with hemodynamics in delta and gamma bands. Another reason for this may be that such associations with scalp EEG were weak and the amount of data we collected did not enable them to achieve statistical significance. The sparseness of the 10-20 coverage did not lend itself to an adequate estimate of the current density through the Laplace montage however inclusion of additional EEG electrodes could provide a local Laplacian estimate to improve space resolution (Nunez and Pilgreen, 1991). The results in Figure 13 dramatically illustrated the fundamentally higher space resolution of fNIRS: the high frequency EEG activity associated with jaw clenching was observed distributed over a wide area whereas the corresponding fNIRS signal was confined to the location of the muscles. Future studies that include EEG source reconstruction and quantitative modeling of the hemodynamic response constrained by data (Boas et al., 2008) will

be helpful in overcoming these limitations. These could be combined with optical image reconstruction, or diffuse optical tomography (Arridge and Schotland, 2009), in order to provide a more robust approach to the investigation of neurovascular coupling.

Another limitation of our study related to the fact that we have not systematically investigated the differences in HRF between subjects. We have also not investigated potential nonstationarities in the HRFs. Preliminary inspection of our data showed evidence of nonstationarity. We did not attempt to separate the contributions to the fNIRS signal of superficial (scalp) and deeper (cortical) components. We used bandpass filtering to remove some physiological artifacts although other more effective (although less practical) methods are available (e.g. Kirilina et al., 2012). The estimated sensitivity to brain tissue of the observed fNIRS signals is ~10% of their total sensitivity (averaged over the 10-20 locations) with a source-detector separation of 30-35 mm (Strangman et al., 2013). Furthermore, our HRF model was linear. In fact it contained only the first set of terms from a more general Volterra expansion (Pouliot, 2012). These shortcomings offer opportunities for further investigation. Our study was part of a broader effort to develop techniques tailored specifically for multi-modal data. Alternatives have been provided in other studies (e.g. Biessmann et al., 2011; Dahne et al., 2013; de Munck et al., 2009).

CONCLUSION

Based on existing literature we expected to find a significant modulation of hemodynamics by alpha rhythms in the posterior cortex but we wished to extend the investigation to the whole-head and the full spectrum of EEG power. In this paper we verified the well-known delayed alpha modulation of hemodynamics in posterior areas. We found an almost equally strong beta power correlation with hemodynamics. Our analysis suggested, however, that the latter was an

artifact of the autocorrelation among EEG rhythms. Signals from the inferior electrode sites were dominated by muscle electrical and oxygenation activity. Our results indicated that whole-head EEG+fNIRS recordings were able to detect patterns of neurovascular coupling over a range of topographic sites and frequencies of neural activity. Our incomplete understanding of neurovascular coupling further highlights the need for widely applicable, light-weight technologies suitable for tracking both the neural and vascular aspects of brain activity under natural conditions. New approaches for accumulating and analyzing hybrid EEG+fNIRS data will be critical for establishing the translational utility of this and other types of multi-modal functional imaging.

ACKNOWLEDGEMENTS

The authors are grateful to Robert Grossman, Marc Garbey, and Dino Dvorak for their helpful criticism during the preparation of the manuscript. Special thanks to Haleh Aghajani for her support in synchronizing the measurement systems. We would also like to thank the Department of Biomedical Engineering and the Cullen College of Engineering at University of Houston for its financial support.

REFERENCES

- Arridge, S.R., and Schotland, J.C. (2009). Optical tomography: forward and inverse problems. *Inverse Probl.* 25, 123010.
- Attwell, D., and Iadecola, C. (2002). The neural basis of functional brain imaging signals. *Trends Neurosci.* 25, 621–625.
- Bari, V., Calcagnile, P., Molteni, E., Re, R., Contini, D., Spinelli, L., Caffini, M., Torricelli, A., Cubeddu, R., Cerutti, S., et al. (2012). From neurovascular coupling to neurovascular cascade: a study on neural, autonomic and vascular transients in attention. *Physiol. Meas.* 33, 1379.
- Berger, H. (1929). Über das elektrenkephalogramm des menschen. *Eur. Arch. Psychiatry Clin. Neurosci.* 87, 527–570.
- Biessmann, F., Plis, S., Meinecke, F.C., Eichele, T., and Muller, K. (2011). Analysis of Multimodal Neuroimaging Data. *Biomed. Eng. IEEE Rev. In* 4, 26–58.
- Boas, D.A., Gaudette, T., Strangman, G., Cheng, X., Marota, J.J., and Mandeville, J.B. (2001). The accuracy of near infrared spectroscopy and imaging during focal changes in cerebral hemodynamics. *Neuroimage* 13, 76–90.
- Boas, D.A., Jones, S.R., Devor, A., Huppert, T.J., and Dale, A.M. (2008). A vascular anatomical network model of the spatio-temporal response to brain activation. *Neuroimage* 40, 1116–1129.
- Britz, J., Van De Ville, D., and Michel, C.M. (2010). BOLD correlates of EEG topography reveal rapid resting-state network dynamics. *Neuroimage* 52, 1162–1170.
- Buccino, A.P., Keles, H.O., and Omurtag, A. (2016). Hybrid EEG-fNIRS Asynchronous Brain-Computer Interface for Multiple Motor Tasks. *PLoS ONE* 11, e0146610.
- Buzsáki, G., and Draguhn, A. (2004). Neuronal oscillations in cortical networks. *Science* 304, 1926–1929.
- Buzsáki, G., Anastassiou, C.A., and Koch, C. (2012). The origin of extracellular fields and currents—EEG, ECoG, LFP and spikes. *Nat. Rev. Neurosci.* 13, 407–420.
- Chatfield, C. (2004). The analysis of time series. *Texts in statistical science* (Chapman & Hall/CRC, Boca Raton, FL).
- Cosandier-Rimélé, D., Bartolomei, F., Merlet, I., Chauvel, P., and Wendling, F. (2012). Recording of fast activity at the onset of partial seizures: Depth EEG vs. scalp EEG. *Neuroimage* 59, 3474–3487.
- Dahne, S., Bielsmann, F., Meinecke, F.C., Mehnert, J., Fazli, S., and Muller, K.-R. (2013). Integration of multivariate data streams with bandpower signals. *Multimed. IEEE Trans. On* 15, 1001–1013.

- Dalal, S.S., Zumer, J.M., Guggisberg, A.G., Trumpis, M., Wong, D.D., Sekihara, K., and Nagarajan, S.S. (2011). MEG/EEG source reconstruction, statistical evaluation, and visualization with NUTMEG. *Comput. Intell. Neurosci.* 2011.
- Delpy, D.T., Cope, M., van der Zee, P., Arridge, S.R., Wray, S., and Wyatt, J.S. (1988). Estimation of optical pathlength through tissue from direct time of flight measurement. *Phys. Med. Biol.* 33, 1433.
- De Munck, J.C., Goncalves, S.I., Huijboom, L., Kuijer, J.P.A., Pouwels, P.J.W., Heethaar, R.M., and da Silva, F.L. (2007). The hemodynamic response of the alpha rhythm: an EEG/fMRI study. *Neuroimage* 35, 1142–1151.
- D'Esposito, M., Deouell, L.Y., and Gazzaley, A. (2003). Alterations in the BOLD fMRI signal with ageing and disease: a challenge for neuroimaging. *Nat. Rev. Neurosci.* 4, 863–872.
- Durduran, T. (2010). Optical measurement of cerebral hemodynamics and oxygen metabolism in neonates with congenital heart defects. *J. Biomed. Opt.* 15.
- Feige, B. (2005). Cortical and subcortical correlates of electroencephalographic alpha rhythm modulation. *J. Neurophysiol.* 93–95.
- Gentili, R.J., Shewokis, P.A., Ayaz, H., and Contreras-Vidal, J.L. (2013). Functional near-infrared spectroscopy-based correlates of prefrontal cortical dynamics during a cognitive-motor executive adaptation task. *Front. Hum. Neurosci.* 7.
- Giacometti, P., and Diamond, S.G. (2013). Compliant head probe for positioning electroencephalography electrodes and near-infrared spectroscopy optodes. *J. Biomed. Opt.* 18, 027005–027005.
- Girouard, H., and Iadecola, C. (2006). Neurovascular coupling in the normal brain and in hypertension, stroke, and Alzheimer disease. *J. Appl. Physiol.* 100–101.
- Goldman, R.I., Stern, J.M., Engel Jr, J., and Cohen, M.S. (2002). Simultaneous EEG and fMRI of the alpha rhythm. *Neuroreport* 13, 2487.
- Goncalves, S.I., De Munck, J.C., Pouwels, P.J.W., Schoonhoven, R., Kuijer, J.P.A., Maurits, N.M., Hoogduin, J.M., Van Someren, E.J.W., Heethaar, R.M., and da Silva, F.L. (2006). Correlating the alpha rhythm to BOLD using simultaneous EEG/fMRI: inter-subject variability. *Neuroimage* 30, 203–213.
- Goncharova, I.I., McFarland, D.J., Vaughan, T.M., and Wolpaw, J.R. (2003). EMG contamination of EEG: spectral and topographical characteristics. *Clin. Neurophysiol.* 114, 1580–1593.
- Grant, A.C., Abdel-Baki, S.G., Weedon, J., Arnedo, V., Chari, G., Koziorynska, E., Lushbough, C., Maus, D., McSween, T., Mortati, K.A., et al. (2014). EEG interpretation reliability and interpreter confidence: a large single-center study. *Epilepsy Behav.* 32, 102–107.
- Greenfield, L.J., Geyer, J.D., and Carney, P.R. (2012). Reading EEGs: a practical approach (Lippincott Williams & Wilkins).

- Huppert, T.J., Hoge, R.D., Diamond, S.G., Franceschini, M.A., and Boas, D.A. (2006). A temporal comparison of BOLD, ASL, and NIRS hemodynamic responses to motor stimuli in adult humans. *Neuroimage* 29, 368–382.
- Huster, R.J., Debener, S., Eichele, T., and Herrmann, C.S. (2012). Methods for simultaneous EEG-fMRI: an introductory review. *J. Neurosci.* 32, 6053–6060.
- Jacques, S.L. (2013). Optical properties of biological tissues: a review. *Phys. Med. Biol.* 58, R37.
- Keles, H.O., Barbour, R.L., Aghajani, H., and Omurtag, A. (2014). Multimodality mapping approach for evolving functional brain connectivity patterns: A fNIRS-EEG study. In *Biomedical Optics*, (Optical Society of America), p. BT5B – 2.
- Kirilina, E., Jelzow, A., Heine, A., Niessing, M., Wabnitz, H., Brühl, R., Ittermann, B., Jacobs, A.M., and Tachtsidis, I. (2012). The physiological origin of task-evoked systemic artefacts in functional near infrared spectroscopy. *Neuroimage* 61, 70–81.
- Kleinschmidt, A. (1996). Simultaneous recording of cerebral blood oxygenation changes during human brain activation by magnetic resonance imaging and near-infrared spectroscopy. *Journal of cerebral blood flow and metabolism : official. J. Int. Soc. Cereb. Blood Flow Metab.* 16–5.
- Koch, S.P., Steinbrink, J., Villringer, A., and Obrig, H. (2006). Synchronization between background activity and visually evoked potential is not mirrored by focal hyperoxygenation: implications for the interpretation of vascular brain imaging. *J. Neurosci.* 26, 4940–4948.
- Koch, S.P., Koendgen, S., Bourayou, R., Steinbrink, J., and Obrig, H. (2008). Individual alpha-frequency correlates with amplitude of visual evoked potential and hemodynamic response. *Neuroimage* 41, 233–242.
- Koch, S.P., Werner, P., Steinbrink, J., Fries, P., and Obrig, H. (2009). Stimulus-induced and state-dependent sustained gamma activity is tightly coupled to the hemodynamic response in humans. *J. Neurosci.* 29, 13962–13970.
- Laufs, H., Kleinschmidt, A., Beyerle, A., Eger, E., Salek-Haddadi, A., Preibisch, C., and Krakow, K. (2003). EEG-correlated fMRI of human alpha activity. *Neuroimage* 19, 1463–1476.
- Len, T.K., and Neary, J.P. (2011). Cerebrovascular pathophysiology following mild traumatic brain injury. *Clin. Physiol. Funct. Imaging* 31, 85–93.
- Lindgren, K.A., Larson, C.L., Schaefer, S.M., Abercrombie, H.C., Ward, R.T., Oakes, T.R., Holden, J.E., Perlman, S.B., Benca, R.M., and Davidson, R.J. (1999). Thalamic metabolic rate predicts EEG alpha power in healthy control subjects but not in depressed patients. *Biol. Psychiatry* 45, 943–952.
- Llinás, R., Ribary, U., Contreras, D., and Pedroarena, C. (1998). The neuronal basis for consciousness. *Philos. Trans. R. Soc. Lond. B Biol. Sci.* 353, 1841–1849.
- Lloyd-Fox, S., Blasi, A., and Elwell, C.E. (2010). Illuminating the developing brain: the past, present and future of functional near infrared spectroscopy. *Neurosci. Biobehav. Rev.* 34, 269–284.

- Logothetis, N.K., and Wandell, B.A. (2004). Interpreting the BOLD signal. *Annu Rev Physiol* 66, 735–769.
- Logothetis, N.K., Pauls, J., Augath, M., Trinath, T., and Oeltermann, A. (2001). Neurophysiological investigation of the basis of the fMRI signal. *Nature* 412, 150–157.
- Malonek, D. (1997). Vascular imprints of neuronal activity: relationships between the dynamics of cortical blood flow, oxygenation, and volume changes following sensory stimulation. In *Proceedings of the National Academy of Sciences of the United States of America*, pp. 94–26.
- Mantini, D., MG, P., C, D.G., GL, R., and Corbetta, M. (2007). Electrophysiological signatures of resting state networks in the human brain. In *Proceedings of the National Academy of Sciences of the United States of America*, pp. 104–132.
- Masamoto, K., and Kanno, I. (2012). Anesthesia and the quantitative evaluation of neurovascular coupling. *Journal of cerebral blood flow and metabolism : official J. Int. Soc. Cereb. Blood Flow Metab.* 32–37.
- Mesquita, R.C., Franceschini, M.A., and Boas, D.A. (2010). Resting state functional connectivity of the whole head with near-infrared spectroscopy. *Biomed. Opt. Express* 1, 324–336.
- Moosmann, M., Ritter, P., Krastel, I., Brink, A., Thees, S., Blankenburg, F., Taskin, B., Obrig, H., and Villringer, A. (2003). Correlates of alpha rhythm in functional magnetic resonance imaging and near infrared spectroscopy. *Neuroimage* 20, 145–158.
- Mukamel, R., Gelbard, H., Arieli, A., Hasson, U., Fried, I., and Malach, R. (2005). Coupling between neuronal firing, field potentials, and fMRI in human auditory cortex. *Science* 309, 951–954.
- de Munck, J.C., Gonçalves, S.I., Mammoliti, R., Heethaar, R.M., and Da Silva, F.L. (2009). Interactions between different EEG frequency bands and their effect on alpha-fMRI correlations. *Neuroimage* 47, 69–76.
- Muthukumaraswamy, S.D. (2013). High-frequency brain activity and muscle artifacts in MEG/EEG: a review and recommendations. *Front. Hum. Neurosci.* 7.
- Niessing, J., Ebisch, B., Schmidt, K.E., Niessing, M., Singer, W., and Galuske, R.A. (2005). Hemodynamic signals correlate tightly with synchronized gamma oscillations. *Science* 309, 948–951.
- Nir, Y., Fisch, L., Mukamel, R., Gelbard-Sagiv, H., Arieli, A., Fried, I., and Malach, R. (2007). Coupling between neuronal firing rate, gamma LFP, and BOLD fMRI is related to interneuronal correlations. *Curr. Biol.* 17, 1275–1285.
- Nunez, P.L., and Pilgreen, K.L. (1991). The spline-Laplacian in clinical neurophysiology: a method to improve EEG spatial resolution. *J. Clin. Neurophysiol.* 8, 397–413.
- Ou, W., Nissilä, I., Radhakrishnan, H., Boas, D.A., Hämäläinen, M.S., and Franceschini, M.A. (2009). Study of neurovascular coupling in humans via simultaneous magnetoencephalography and diffuse optical imaging acquisition. *NeuroImage* 46, 624–632.

- Petroff, O.A., Spencer, D.D., Goncharova, I.I., and Zaveri, H.P. (2015). A comparison of the power spectral density of scalp EEG and subjacent electrocorticograms. *Clin. Neurophysiol.*
- Pfurtscheller, G., Stancak, A., and Neuper, C. (1996). Event-related synchronization (ERS) in the alpha band—an electrophysiological correlate of cortical idling: a review. *Int. J. Psychophysiol.* *24*, 39–46.
- Pouliot, P. (2012). Nonlinear hemodynamic responses in human epilepsy: a multimodal analysis with fNIRS-EEG and fMRI-EEG. *J. Neurosci. Methods* *204*–2.
- Proulx, S., Safi-Harb, M., LeVan, P., An, D., Watanabe, S., and Gotman, J. (2014). Increased sensitivity of fast BOLD fMRI with a subject-specific hemodynamic response function and application to epilepsy. *NeuroImage* *93*, 59–73.
- Ritter, P., Moosmann, M., and Villringer, A. (2009). Rolandic alpha and beta EEG rhythms' strengths are inversely related to fMRI-BOLD signal in primary somatosensory and motor cortex. *Hum. Brain Mapp.* *30*, 1168–1187.
- Roche-Labarbe, N., Zaaimi, B., Berquin, P., Nehlig, A., Grebe, R., and Wallois, F. (2008). NIRS-measured oxy-and deoxyhemoglobin changes associated with EEG spike-and-wave discharges in children. *Epilepsia* *49*, 1871–1880.
- Sadaghiani, S., Scheeringa, R., Lehongre, K., Morillon, B., Giraud, A.-L., and Kleinschmidt, A. (2010). Intrinsic connectivity networks, alpha oscillations, and tonic alertness: a simultaneous electroencephalography/functional magnetic resonance imaging study. *J. Neurosci.* *30*, 10243–10250.
- Safaie, J., Grebe, R., Moghaddam, H.A., and Wallois, F. (2013). Toward a fully integrated wireless wearable EEG-NIRS bimodal acquisition system. *J. Neural Eng.* *10*, 056001.
- Scholkmann, F., Kleiser, S., Metz, A.J., Zimmermann, R., Pavia, J.M., Wolf, U., and Wolf, M. (2014). A review on continuous wave functional near-infrared spectroscopy and imaging instrumentation and methodology. *NeuroImage* *85*, 6–27.
- Schomer, D.L., and Da Silva, F.L. (2012). Niedermeyer's electroencephalography: basic principles, clinical applications, and related fields (Lippincott Williams & Wilkins).
- Sirotin, Y.B., and Das, A. (2009). Anticipatory haemodynamic signals in sensory cortex not predicted by local neuronal activity. *Nature* *457*, 475–479.
- Sirovich, L., Omurtag, A., and Lubliner, K. (2006). Dynamics of neural populations: Stability and synchrony. *Netw. Comput. Neural Syst.* *17*, 3–29.
- Srinivasan, R., WR, W., Ding, J., and PL, N. (2007). EEG and MEG coherence: measures of functional connectivity at distinct spatial scales of neocortical dynamics. *J. Neurosci. Methods* *166*–1.
- Steinbrink, J., Villringer, A., Kempf, F., Haux, D., Boden, S., and Obrig, H. (2006). Illuminating the BOLD signal: combined fMRI–fNIRS studies. *Magn. Reson. Imaging* *24*, 495–505.

- Steriade, M. (2001). Impact of network activities on neuronal properties in corticothalamic systems. *J. Neurophysiol.* 86–1.
- Steriade, M. (2006). Grouping of brain rhythms in corticothalamic systems. *Neuroscience* 137, 1087–1106.
- Strangman, G., Culver, J.P., Thompson, J.H., and Boas, D.A. (2002). A quantitative comparison of simultaneous BOLD fMRI and NIRS recordings during functional brain activation. *Neuroimage* 17, 719–731.
- Strangman, G.E., Li, Z., and Zhang, Q. (2013). Depth sensitivity and source-detector separations for near infrared spectroscopy based on the Colin27 brain template. *PloS One* 8, e66319.
- Tyvaert, L., LeVan, P., Grova, C., Dubeau, F., and Gotman, J. (2008). Effects of fluctuating physiological rhythms during prolonged EEG-fMRI studies. *Clin. Neurophysiol.* 119, 2762–2774.
- Uglialoro, A. (2014). Cerebral Monitoring and Surveillance Using High-Resolution Functional Optical Imaging. *Neurovascular Coupling Methods, Neuromethods*, eds Zhao. M Ma H Schwartz TH Springer N. Y. Vol 88, 307–330.
- Van Drongelen, W. (2006). Signal processing for neuroscientists: an introduction to the analysis of physiological signals (Academic Press).
- Varela, F., Lachaux, J.-P., Rodriguez, E., and Martinerie, J. (2001). The brainweb: phase synchronization and large-scale integration. *Nat. Rev. Neurosci.* 2, 229–239.
- White, B.R., Snyder, A.Z., Cohen, A.L., Petersen, S.E., Raichle, M.E., Schlaggar, B.L., and Culver, J.P. (2009). Resting-state functional connectivity in the human brain revealed with diffuse optical tomography. *Neuroimage* 47, 148–156.
- Whitham, E.M., Pope, K.J., Fitzgibbon, S.P., Lewis, T., Clark, C.R., Loveless, S., Broberg, M., Wallace, A., DeLosAngeles, D., Lillie, P., et al. (2007). Scalp electrical recording during paralysis: quantitative evidence that EEG frequencies above 20Hz are contaminated by EMG. *Clin. Neurophysiol.* 118, 1877–1888.
- Worsley, K.J., Liao, C.H., Aston, J., Petre, V., Duncan, G.H., Morales, F., and Evans, A.C. (2002). A general statistical analysis for fMRI data. *Neuroimage* 15, 1–15.
- Wu, L., Eichele, T., and Calhoun, V.D. (2010). Reactivity of hemodynamic responses and functional connectivity to different states of alpha synchrony: a concurrent EEG-fMRI study. *Neuroimage* 52, 1252–1260.
- Xu, Y., Gruber, H.L., Barbour, R.L., Blanco, I., Zirak, P., Fortuna, A., Cotta, G., Mayos, M., Mola, A., Durduran, T., et al. (2014). nirsLAB: A Computing Environment for fNIRS Neuroimaging Data Analysis. In *Biomedical Optics*, (Optical Society of America), p. BM3A – 1.